Materials Research. 2026; 29: e20250740
DOI: https://doi.org/10.1590/1980-5373-MR-2025-0740

Aluminum Composites with Graphene Oxide: Comparing Liquid-Phase Mixing Methods

Rodolfo L. P. Gonçalves[a]*, Dolores Lazar[b], Rubens N. Faria[b], Rafael E. Cubi[a], Roberto S. Jr.[c], Lucas S. Peres[c], Marcos Massi[a], Antônio A. Couto[a]

[a]Universidade Presbiteriana Mackenzie, Escola de Engenharia, Programa de Pós-Graduação em Engenharia de Materiais e Nanotecnologia (PPGEMN), São Paulo, Brasil.
[b]Instituto de Pesquisas Energéticas e Nucleares (IPEN), Centro de Ciência e Tecnologia dos Materiais (CCTM), São Paulo, SP, Brazil.
[c]Companhia Brasileira de Alumínio (CBA), Alumínio, SP, Brasil.

Received: December 05, 2025; Revised: April 16, 2026; Accepted: May 04, 2026

In the manufacture of graphene-reinforced aluminum composites, powder metallurgy has been the primary production method, proving to be highly effective. The present work addresses the production and characterization of aluminum matrix composites reinforced with graphene-based nanomaterials. The production route employed the powder metallurgy technique and was processed in two stages: first by mixing in different liquid media, and second by using distinct mixing methods. The sintered samples from the first stage were evaluated for their density, and the sintered samples from the second stage were subjected to mechanical microhardness tests. The results of the first stage indicated that among the solvents used for mixing, acetone and ethanol stood out, providing compacts with densification above 92%. In the second stage, Al/rGr composite samples produced by the mechanical mixing method using a helical impeller showed the greatest increase in hardness, achieving a 60.5% increase compared to pure aluminum.

Keywords: *graphene, aluminum powder, composite, powder metallurgy*

1. Introduction

Graphene, owing to its exceptional mechanical properties, such as a Young's modulus of 1.0 TPa and a high fracture strength of approximately 130 GPa[1] , is an extremely promising reinforcement material in metal matrix composites. The mechanical properties of metallic matrices such as Cu[2], Mg[3], and Ti[4] could be improved. These enhancements are primarily attributed to effective load transfer at the matrix–reinforcement interface and the homogeneous dispersion of graphene-based materials.

Among metallic matrices, aluminum and its alloys stand out as prime candidates for graphene-based reinforcement due to their low density, low melting point, excellent versatility, and favorable cost–benefit ratio. Previous studies have reported substantial improvements in mechanical performance with the incorporation of graphene. Wang et al.[5] achieved a 62% increase in tensile strength compared to pure aluminum by employing a flake powder metallurgy (Flake PM) method[6].

This method involved introducing a hydrophilic polyvinyl alcohol (PVA) membrane onto the surface of aluminum flakes and adding deionized water to form a powder paste, into which an aqueous dispersion of graphene oxide (GO) was subsequently incorporated. The mixed paste was mechanically agitated and heated at 550 °C for 2 hours to decompose the PVA and reduce the GO nanosheets to graphene nanosheets (GNSs).

Similarly, Gao et al.[7] reported a 30% increase in ultimate tensile strength by mixing pure aluminum in an aqueous solution containing the cationic surfactant hexadecyl trimethylammonium bromide (CTAB), followed by mechanical agitation with an aqueous dispersion of GO that had been pre-treated by 1 hour of ultrasonication. Furthermore, enhancements in flexural strength of up to 47% have been reported for Al6061 alloy[8] using a ball milling high energy method, with an evaluation of the effects of milling time and graphene content, while Pérez-Bustamante et al.[9], also employing ball milling high energy and a detailed analysis of the influence of milling time and graphene percentage, observed a maximum increase in microhardness of 138%.

Another significant study demonstrated an improvement of up to 80% in compressive strength[10] by using an aqueous suspension preparation route with the addition of Mg^{2+} ions as a binding agent, which promoted stronger affinity and adhesion of graphene sheets to the surface of aluminum particles, resulting in a more homogeneous and effective dispersion of the reinforcement. Although these results underscore the potential of aluminum–graphene composites for applications in the aerospace, aeronautical, and automotive industries[11], they also highlight the critical need to optimize fabrication methods, particularly regarding the uniform dispersion of the reinforcement, sintering steps, and the preservation of graphene's structural integrity.

*e-mail: rodolfo.goncalves@mackenzie.br
Associate Editor: Aloisio Klein.
Editor-in-Chief: Luiz Antonio Pessan.

Among the available methods for fabricating graphene-reinforced aluminum composites, solid-state processing via powder metallurgy is the most widely adopted. This method enables lower processing temperatures compared to techniques that employ the liquid state, thereby minimizing undesirable and deleterious interfacial reactions such as the formation of Al_4C_3[9,12]. Despite these advantages, powder metallurgy still faces significant challenges during the mixing stage, such as ensuring homogeneous dispersion of graphene and preventing its agglomeration due to density differences and van der Waals interactions between graphene sheets. Recent review articles emphasize these challenges, noting that achieving a strong matrix–reinforcement interface and a uniform distribution of graphene remain major unresolved issues[13]. Chak and Chattopadhyay[14] specifically highlight that improvements in mechanical properties depend strongly on the effective dispersion of graphene, associating agglomeration phenomena with premature mechanical failures in the composites.

Given these persistent dispersion challenges in solid-state processing, liquid-phase strategies are increasingly explored as they offer a pathway to potentially deagglomerate graphene-based materials more effectively prior to consolidation. The use of graphene oxide (GO) or reduced graphene oxide (rGO), with their surface functional groups, can be particularly advantageous in liquid media, promoting better wettability and interaction with solvents, which is crucial for breaking down agglomerates and achieving finer dispersion with aluminum particles[15]. Nevertheless, the transition from a dispersed liquid system to a solid composite precursor is not trivial; issues such as re-agglomeration during solvent evaporation, the choice of solvent affecting GO/rGO stability and interaction with Al, and the potential for residual solvent contamination or unwanted reactions during drying or sintering must be carefully managed[16]. Moreover, ensuring that the improved dispersion achieved in the liquid phase translates into enhanced interfacial bonding and load transfer in the final sintered composite remains a key objective that requires careful process control[17].

However, typically, the mixing process for aluminum–graphene composites in powder metallurgy involves pre-synthesized aluminum powder combined with graphene via two main routes: dry mixing such as ball milling using different systems (agitator[8], attritor[12,18] or planetary mill[19,20]) or liquid mixing routes (mechanical stirring[21,22], ultrasonication[23,24], liquid dispersion[25] or rotary evaporation[26]). Critical evaluations of these methods discussed in recent reviews[13] reveal that, despite the variety of available mixing techniques, there is still no consensus on the ideal method that simultaneously ensures homogeneous dispersion and the preservation of graphene's intrinsic properties. Furthermore, specific aspects such as the effectiveness of load transfer at the matrix–reinforcement interface remain to be fully explored.

The objectives motivated by this present work aim to systematically investigate aluminum composites reinforced with graphene oxide (GO) and reduced graphene oxide (rGO) produced via a two-step powder metallurgy process, showing the differences between these two mechanisms.

2. Materials and Methods

The aluminum powder utilized in this study, provided by Alfa Aesar, had a purity of 99.5% and an average particle size of 45 μm, as per the manufacturer's specifications. Two distinct carbon-based materials, supplied by ACS Material, were independently used as reinforcements for the composites: reduced graphene oxide (rGO) and graphene oxide (GO). The material's specifications, as provided by the manufacturer, are listed in Table 1.

At first, aluminum powders were mixed with GO using various liquid dispersion media—water, acetone, ethanol, and an ethanol/water mixture (40/60)—to identify the optimal solvent that minimizes graphene agglomeration by reducing the attractive forces between its sheets. Subsequently, using the optimal liquid medium identified in the first stage, different mixing techniques were comparatively evaluated in terms of dispersion homogeneity and the preservation of graphene's intrinsic properties. The resulting composites were characterized by microhardness testing, Raman spectroscopy, X-ray diffraction (XRD), and electron microscopy, with the aim of establishing a systematic correlation between the dispersion and structural integrity of graphene and the adopted processing conditions (Figure 1).

Table 1. Characteristics of rGO and GO provided by ACS Material.

Characteristics of rGO	
Preparation Method	Modified Hummer's Method followed by thermal exfoliation + hydrogen reduction.
Diameter	0.4 ~ 5 μm
Thickness	0.6 ~ 1.2 nm
BET Surface Area (m^2/g)	400 ~ 1000
Electrical Resistivity (Ω.cm)	≤ 0.30
Density	~ 0.01 g/cm^3
Dispersibility Property	Can be redispersed in most solvents with the aid of sonication
Characteristics of GO	
Preparation Method	Modified Hummer's Method
Diameter	1 ~ 5 μm
Thickness	0.8 ~ 1.2 nm
Single-Layer Proportion	~80%
Purity	~ 99%
Bulk Density	0.26 g/cm^3

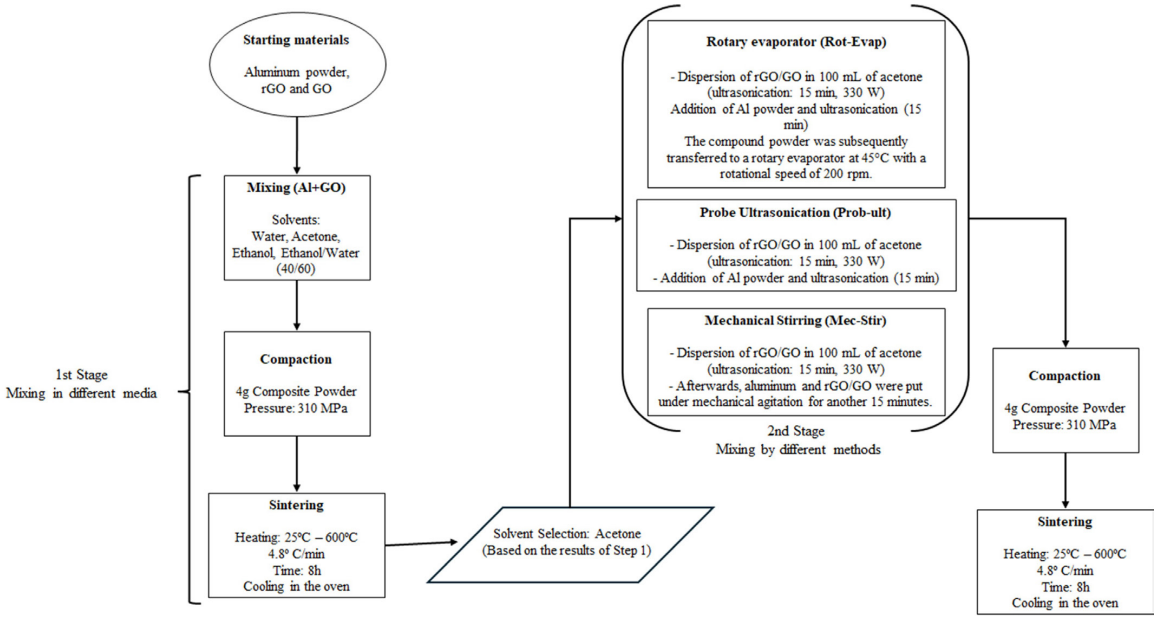

Figure 1. Process Flowchart.

In the first step, pure aluminum powder and GO were mixed with solvents:

- water,
- acetone,
- pure ethanol,
- 40/60 ethanol-water mixture.

Composites containing 0.3 wt% GO were prepared, following proportions proven effective in previous studies[5,7]. Aluminum powder was dispersed in 50 mL of each solvent and ultrasonicated for 30 minutes, while GO was separately dispersed in 30 mL of the same solvents under identical conditions. The mixtures were then combined according to their respective solvents and subjected to another 30 minutes of ultrasonication. Finally, the suspensions were dried in an oven for 24 hours. One of the alcohol suspensions was dried in vacuum.

In the second step, 4 g of pure aluminum powder was mixed with 0.3 wt% of rGO 0.3 wt% or GO using various mixing techniques. The equipment utilized included a BUCHI R-100 rotary evaporator with a vacuum pump and I-100 interface, an Eco-Sonics QR550 ultrasonic probe sonicator, and an IKA RW20.N mechanical stirrer with a helical impeller.

In the rotary evaporator dispersion process (referred to here as *Rot-Evap*), rGO was first dispersed in 100 mL of acetone using a probe ultrasonicator operating at 20 kHz with a 13 mm tip. The sonication was performed at 60% power (330 W) for 15 minutes. Aluminum powder was then added to the mixture, and agitation continued for an additional 15 minutes, totaling 30 minutes of processing. The composite powder was subsequently transferred to a rotary evaporator, where mixing and drying were carried out simultaneously at 45°C with a rotation speed of 200 rpm.

In the dispersion process using probe ultrasonication (referred to here as *Prob-Ult*), rGO was dispersed in 100 mL of acetone with a 20 kHz ultrasonic probe featuring a 13 mm tip. The dispersion was conducted at 60% power (330 W) for 15 minutes. Subsequently, aluminum powder was introduced into the mixture while agitation was maintained for another 15 minutes, completing a total processing time of 30 minutes. The resulting mixture was then oven-dried at 54°C for 24 hours.

In the mechanical stirring process (referred to here as *Mec-Stir*), rGO was first dispersed in 100 mL of acetone using a probe ultrasonicator at 20 kHz with a 13 mm tip, operating at 60% power (330 W) for 15 minutes. At the same time, aluminum powder was stirred in acetone with a helical impeller at 1000 rpm for 15 minutes. Afterward, the ultrasonicated graphene was combined with the aluminum under mechanical stirring, and the mixture was agitated for another 15 minutes, totaling 30 minutes of processing. The resulting mixture was then oven-dried at 54°C for 24 hours. The same processes were also carried out with GO.

In both stages, pellets were formed using cold uniaxial pressing at a pressure of approximately 310 MPa for a duration of 60 seconds. About 4 grams of composite powder aluminum with 0.3 wt% rGO or GO were placed into a steel die with a diameter of 20 mm. The die was pre-lubricated with stearic acid to facilitate the compaction process.

Samples from both processing stages were sintered in a tubular furnace under a nitrogen atmosphere, starting from ambient temperature (25°C). The temperature was raised to 600°C at a heating rate of 4.8°C/min, taking about 2 hours to reach the target temperature. Once at 600°C, the samples were held at this temperature for 6 hours, resulting in a total sintering duration of 8 hours. After the sintering process, the nitrogen flow was discontinued, and the samples were allowed to cool inside the furnace to room temperature.

To characterize the samples from the initial stage, the density and degree of densification of the green specimens were assessed using geometric density calculations.

Samples were prepared for analysis by grinding the samples using a variable-speed grinder-polisher equipped with water-lubricated sandpapers of grit sizes 300, 400, 600, and 1200. Following grinding, mechanical polishing was employed to remove surface imperfections and enhance the finish, utilizing a 1 μm diamond paste.

Material characterization involves multiple techniques. A JEOL JSM-6701F scanning electron microscope (SEM) was used for imagining the samples. Optical microscopy was performed alongside Raman spectroscopy using a 100× objective lens. For X-ray diffraction (XRD) analysis, a Rigaku MiniFlex diffractometer with a copper X-ray tube (Cu Kα radiation, λ = 1.542 Å) was utilized. XRD scans were conducted in grazing incidence mode with an incidence angle of 1°, covering a 2θ range from 5° to 90°, at a scanning speed of 10° per minute, a step size of 0.01°, and operating conditions of 40 kV and 15 mA.

A WiTec 300R spectrophotometer featuring a 488 nm He-Ne laser was employed for spectroscopic analysis. Point measurements were taken within the samples to verify the presence of reduced graphene oxide and graphene oxide after processing.

Microhardness (HV0.5) testing was performed on the pellets produced via different mixing methods using a Zwick microhardness tester. The tests were conducted with a 50× objective lens and a diamond indenter under a load of 4.9 N, assessing 25 randomly selected points within each sample.

For each sample, 25 measurements were taken at random points, and this process was performed in triplicate. The mean and standard deviation were calculated from these datasets, allowing for quantification of the central tendency and variability of the measured properties. Although simple, this approach ensures that the differences observed between the samples are both representative and reliable, contributing to a robust interpretation of the results presented.

3. Results and Discussion

3.1. Composites produced in different media

Table 2 presents the results of relative density (densification) obtained from the mixtures prepared in different media.

Table 2 indicates that among the various mixing media for aluminum powder with GO, pure ethanol, acetone, and pure ethanol (vacuum-dried) were the most effective for composite fabrication, as they achieved sintered densities above 90% and showed a positive increase in relative density. When the mixing medium contains water, a lower green density of the samples is observed compared to all the others, along with a negative percentage in relative density (-5.7%), suggesting that the material expanded. This phenomenon can be attributed to the hydrolysis reactions (1) and (2) occurring between aluminum and water.

$$2Al_{(s)} + 6H_2O_{(l)} \rightarrow 2Al(OH)_{3(s)} + 3H_{2(g)} \quad (1)$$

$$2Al_{(s)} + 4H_2O_{(l)} \rightarrow 2AlO(OH)_{(s)} + 3H_{2(g)} \quad (2)$$

Studies[27] indicate that cavitation generated during ultrasonication can induce microstructural changes in metal particles, including the mechanical disruption of the passive oxide layer, thereby exposing the aluminum to water. In aluminum-water systems at temperatures below 35°C, aluminum remains inert. However, when the system temperature rises to 45°C or higher, the reaction initiates, leading to the production of significant amounts of hydrogen through the hydrolysis of aluminum[28]. The collapse of cavitation-induced bubbles within the liquid, during the ultrasonication process, generates high pressures and localized temperatures facilitate these reactions between aluminum and water.

Figure 2 shows scanning electron microscopy (SEM) images of composite powders processed in different media (water, acetone, and ethanol), as well as pure aluminum powder in its as-received state, along with the XRD pattern corresponding to the composite powder processed in water.

Figure 2 shows $Al(OH)_3$ structures formed due to the hydrolysis of aluminum. This occurrence is consistent with the findings of Zhang et al.[29]. Furthermore, Wang et al.[30] observed comparable results in their study on the generation of hydrogen as a byproduct of the reaction between aluminum and deionized water. The XRD patterns corresponding to Figures 1a and 1b exhibit characteristic peaks of $Al(OH)_3$, which were also identified in the studies by Wang et al.[30] and Zhang et al.[31].

The presence of $Al(OH)_3$ on the surface of the particles hinders the compaction process, reducing sliding and interlocking between aluminum particles, in addition to limiting plastic deformation. This explains the lower green density of the samples processed with water.

In the sintering phase we have the decomposition of aluminum hydroxide and oxyhydroxide in alumina. Studies[32,33] discuss in detail the heat treatment of $Al(OH)_3$ and AlO(OH), highlighting the various crystalline phase transformations that occur as a function of the calcination temperature. In the temperature range between 250°C and 500°C, these conditions are sufficient to dehydrate aluminum hydroxides and oxyhydroxides, forming an intermediate Al_2O_3 phase[34] and releasing water vapor, as described in reactions (3) and (4).

Table 2. Results Obtained from Mixtures in Different Media.

	Average Relative Density (%)		
Composites produced	Green	Sintered	Density Increase (%)
Al/0.3 wt% GO - Water	73.06	-	-
Al/0.3 wt% GO - Acetone	92.58	94.31	1.87
Al/0.3 wt% GO - Pure Ethanol	90.94	93.94	3.29
Al/0.3 wt% GO - Ethanol/Water (40/60)	78.40	73.92	-5.71
Al/0.3 wt% GO - Pure Ethanol (Vacuum)	92.25	93.49	1.35
Pure Al	93.15	95.19	2.20

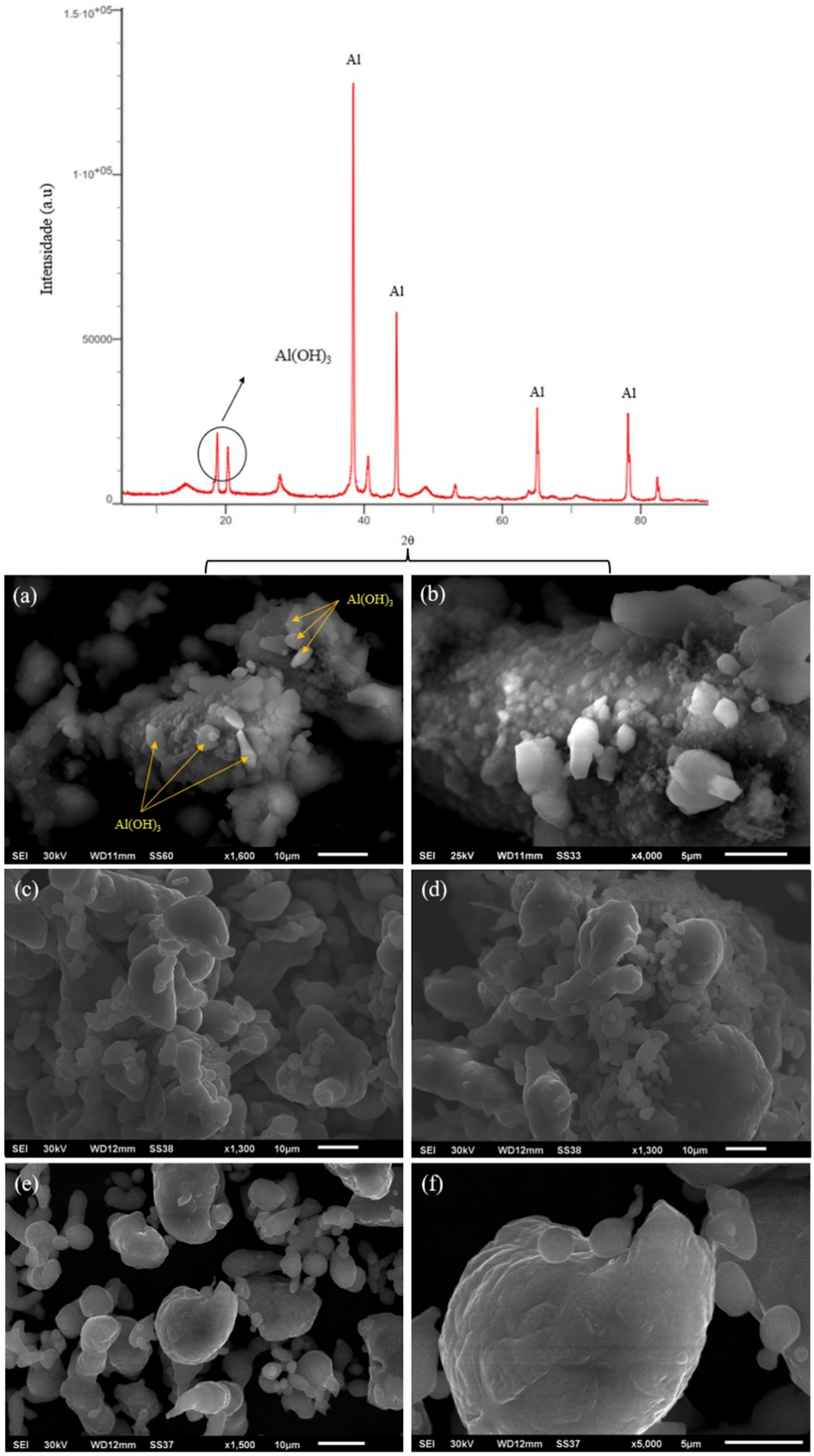

Figure 2. XRD pattern of the composite powder mixed in water and SEM images of the composite powder: (a, b) processed in water; (c) processed in acetone; (d) processed in ethanol; (e, f) pure aluminum as received.

$$2Al(OH)_{3(s)} \xrightarrow{\Delta} Al_2O_{3(s)} + 3H_2O_{(g)} \quad (3)$$

$$2AlO(OH)_{(s)} \xrightarrow{\Delta} Al_2O_{3(s)} + H_2O_{(g)} \quad (4)$$

Aluminum can expand during sintering due to two phenomena: expansion by gases trapped in closed pores during compaction; or gases from chemical reactions diffusing into closed pores. These phenomena are also observed in copper and discussed by Hao et al.[35]. During sintering at 600ºC of the Al/GO composites mixed in water, the conditions were very favorable for the decomposition of $Al(OH)_3$ and AlO(OH), resulting in the release of water vapor, causing expansion of the compacts, impairing the sintering mechanisms and promoting low densification and structural fragility.

As the first stage of evaluation between different media was restricted to the final density characteristics of the sintered composite, both acetone and ethanol proved to be excellent candidates for the second stage, as both mixing media provided a sintered composite with densities above 90%.

3.2. Composites produced using different mixing methods

A comparison of the XRD patterns for composites produced via different graphene incorporation methods is shown in Figure 3, revealing the impact of the synthesis route on the material's structure.

In Figure 3, the characteristic peaks of aluminum can be identified at 2θ ≈ 38°, 44°, 65°, 78°, and 82°, according to JCPDS #65-2869. Additionally, the peaks for rGO appear at 2θ ≈ 24° (broad peak) and 43°[36,37], indicating that GO underwent reduction during processing. This reduction may have occurred both in the mixing stage and in the sintering stage. During the mixing process, once the passive oxide layer on aluminum is disrupted, the exposed aluminum generates Al^{3+} (= -1,66 V)[38], which attract the negatively charged GO through electrostatic forces[39,40]. This interaction partially reduces the GO and facilitates its adsorption onto the aluminum surface.

Asgharzadeh et al.[21] observed a similar phenomenon when they mixed aluminum powder with GO in ethanol using magnetic stirring. Similarly, Li et al.[41] and Fan et al.[42] reported comparable reduction mechanisms, with their XRD results showing rGO peaks consistent with those seen in Figure 3. Intense fluid motion during sonication in the mixing phase induces collisions between particles and with the container walls, potentially removing functional groups from the basal plane of GO[43]. Soltani et al.[44] observed that the collapse of short-lived cavitation bubbles releases localized energy sufficient to drive the reduction of GO. Additionally, radicals generated during sonication further facilitate this reduction process[45]. Zhang et al.[46] and Krishnamoorthy et al.[47] both highlight the efficiency of sonochemical treatment in converting GO to rGO.

During sintering, reduction of GO may also have occurred. Yan et al.[48] investigated CO_2 emissions from Al/GNF composites sintered at 480 °C, confirming that thermal reduction can occur at relatively moderate temperatures. Supporting evidence from other studies[49,50] strongly suggests that the sintering process at 600 °C played a crucial role in the reduction of GO.

All samples exhibited a peak at 2θ ≈ 31°, likely corresponding to Al_4C_3, in agreement with earlier research[51,52]. Additionally, the peak at 2θ ≈ 26.5° is attributed to graphite. Several minor peaks remain unassigned, though some align with aluminum oxide phases.

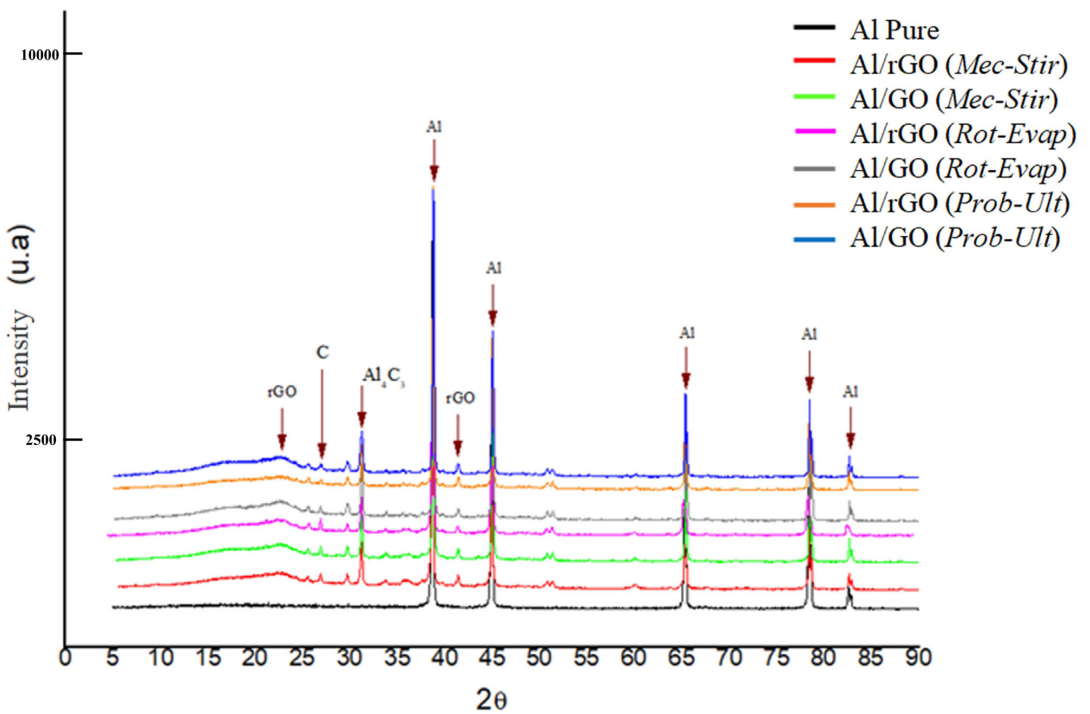

Figure 3. XRD Patterns of Al/rGO and Al/GO composites produced using different mixing methods.

Raman spectroscopic analysis was conducted through point measurements at selected locations of the sintered samples. The primary objective of this approach was qualitative, focusing on verifying the presence and investigating the local structural characteristics of graphene oxide (GO) and reduced graphene oxide (rGO) incorporated into the aluminum matrix after the distinct mixing and sintering processes. Figures 4 and 5 show, respectively, the Raman spectra of Al/rGO and Al/GO composites produced by: mechanical stirring (4a and 5a), rotary evaporation (4b and 5b), and ultrasonication (4c and 5c).

Firstly, the dark contrasts observed are pores and other surface defects, such as scratches resulting from cutting and polishing, observed in all of the images shown. The spectra of all the samples show the D band at approximately 1367 cm^{-1} and the G band near 1614 cm^{-1}. Interestingly, the G band at around 1620 cm^{-1}, which is typically associated with graphite[53,54], may also signify the presence of intercalation compounds[55] or oxidized sp^2 carbon[56]. In reduced graphene oxide, the G band generally appears between ~1580 and ~1600 cm-[1], influenced by the oxidation state and structural organization. In graphene-based materials, a peak at approximately 1620 cm^{-1}, known as the D' band, is indicative of significant structural disorder or defects[57].

Bartolucci et al.[12] observed the formation of Al_4C_3 in aluminum composites reinforced with thermally reduced graphene oxide, attributing this to high processing temperatures and growth along high-energy prismatic planes, suggesting that Al_4C_3 nucleates at defect sites within graphitic planes or amorphous carbon coatings, which could explain the characteristic peaks observed in the XRD pattern shown in Figure 3.

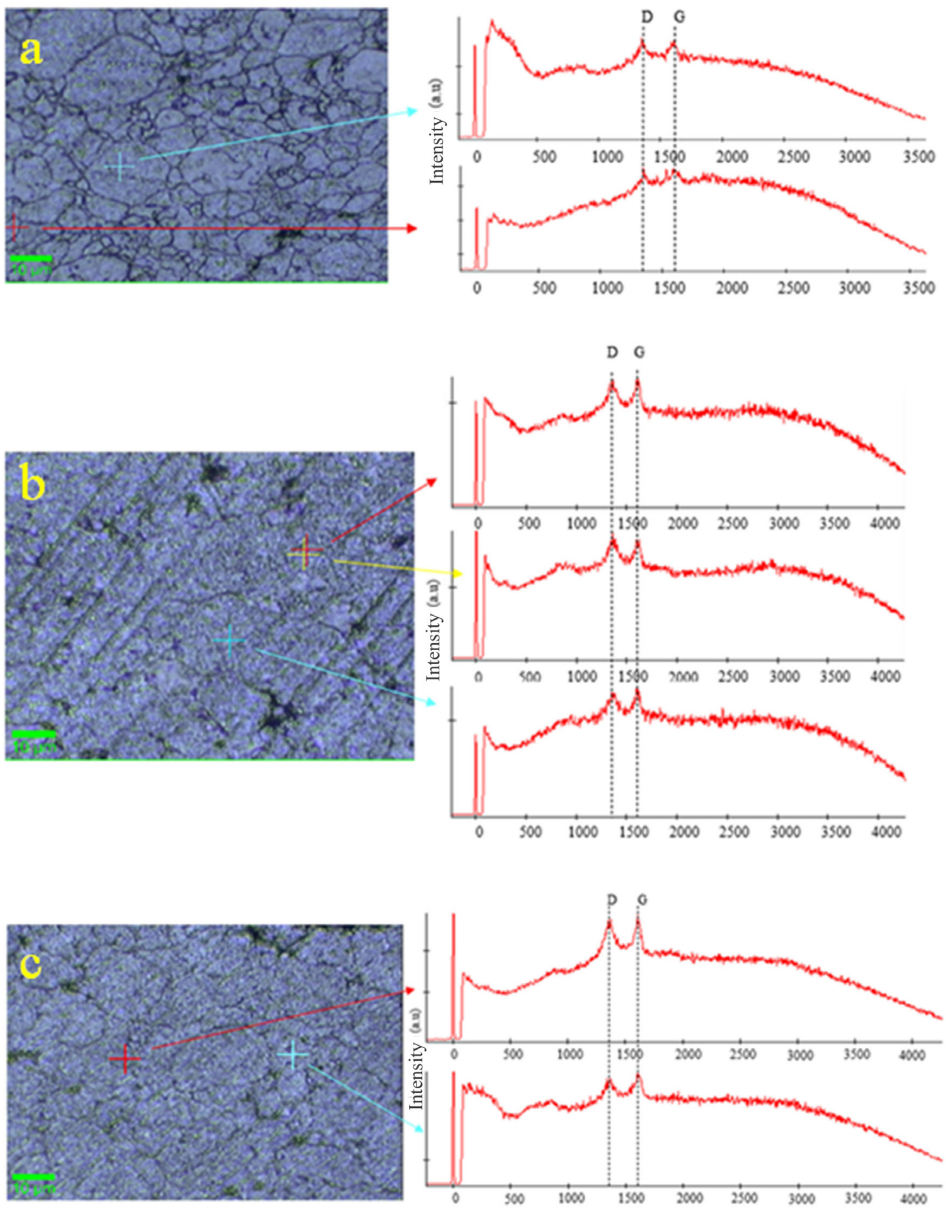

Figure 4. Raman Spectra of Al/rGO composite produced by: (a) Mechanical Stirring, (b) Rotary Evaporation, and (c) Ultrasonication.

Li et al.[58] comment that the Al_4C_3 phase is extremely detrimental to the tensile properties of the composite, where interfacial occurrence also damages the properties of the graphene itself. However, there is an incomplete understanding of the mechanisms for the formation of Al_4C_3, which are related to the shape, size and location of this interfacial composite formation, since they are strongly associated with process methods and parameters; in addition to little clarification on charge transfer[51].

Table 3 presents the microhardness (HV0.5) results, and the percentage increase compared to the pure aluminum samples.

According to Table 3, the Al/rGO composite produced by mechanical stirring demonstrated a remarkable 60.5% increase in microhardness compared to pure aluminum, differentiating it from the other samples. Although all composites showed better performance than pure aluminum, those with less than 10% improvement are considered insignificant due to the measured standard deviation, indicating that the dislocation density in these composites is close to that of pure aluminum. This minimal improvement can be attributed to inadequate dispersion or agglomeration and reduction in lateral dimensions of rGO and GO during processing.

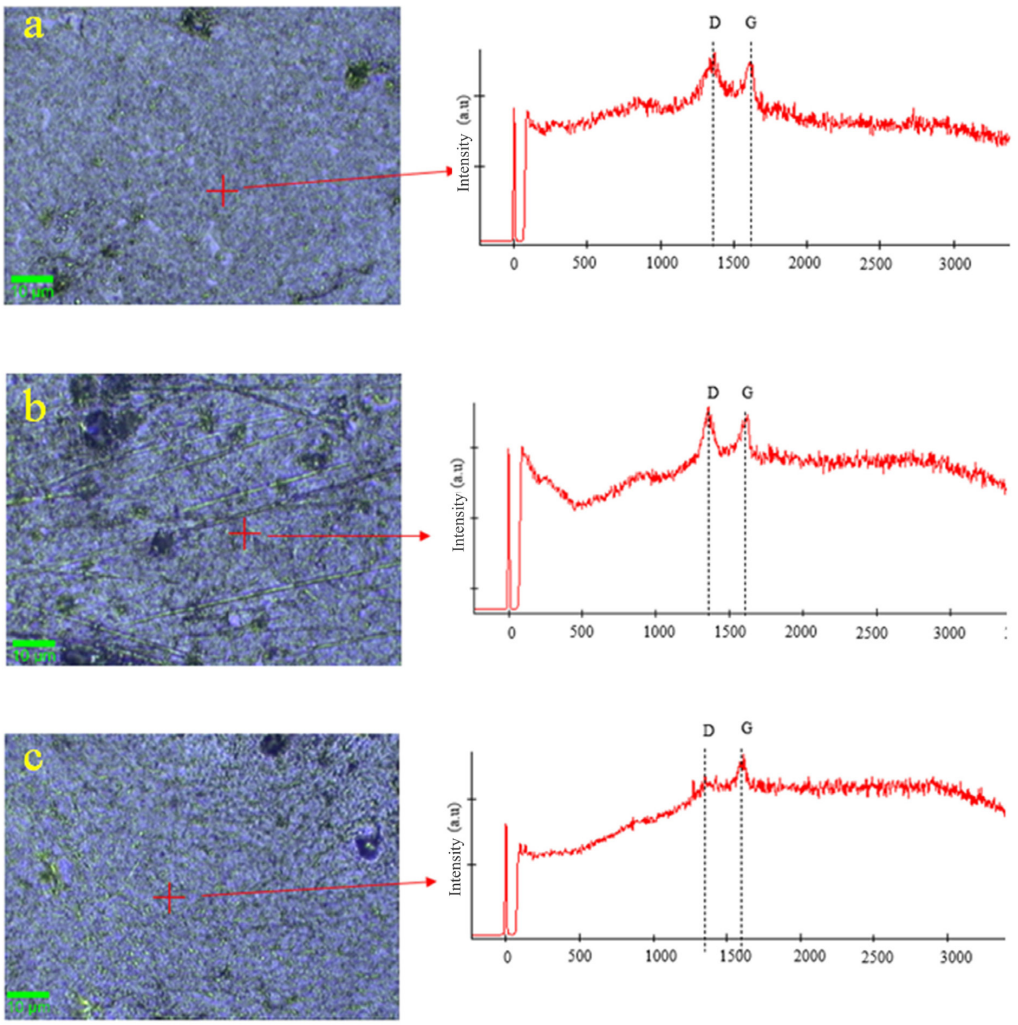

Figure 5. Raman Spectra of Al/GO composite produced by: (a) Mechanical Stirring, (b) Rotary Evaporation, and (c) Ultrasonication.

Table 3. Microhardness (HV0.5) and Percentage Increase of Composites Compared to the Pure Aluminum Sample.

Sample	Average (HV0.5)	Microhardness Increase (%)
Al pure	39.0 ± 1.5	-
Al/rGO (*Prob-Ult*)	39.7 ± 4.3	+1.7
Al/rGO (*Rot-Evap*)	45.2 ± 3.5	+15.9
Al/rGO (*Mec-Stir*)	62.6 ± 12.2	+60.5
Al/GO (*Prob-Ult*)	40.3 ± 2.8	+3.4
Al/GO (*Rot-Evap*)	41.9 ± 3.0	+7.4
Al/GO (*Mec-Stir*)	42.1 ± 4.1	+8.0

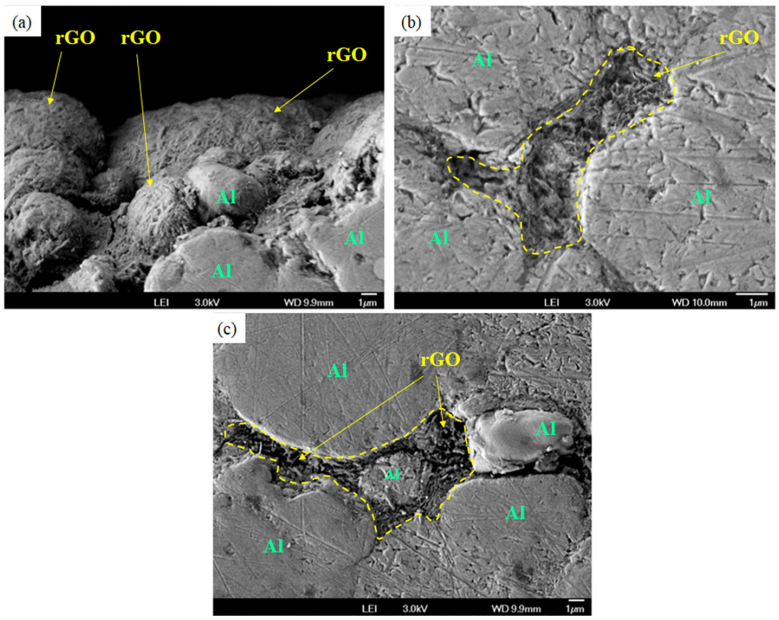

Figure 6. FEG-SEM of Al/rGO Composite (*Mec-Stir*): (a) particles coated with rGO; (b) and (c) regions with rGO agglomerates at aluminum grain boundaries.

Ultrasonication-induced dispersions can lead to a decrease in sp^2 domains and particle size of rGO or GO, as well as promote the formation of edge defects. This effect was observed by Baig et al.[59] when studying the influence of tip ultrasonication on the structural quality of graphene nanoplatelets.

Significantly, only the Al/rGO composite processed by mechanical stirring showed a substantial improvement in microhardness. One possible reason is that during mechanical agitation, both GO and rGO were exposed to ultrasound for a shorter period of time, 15 min during initial dispersion to break the powder state, compared to 30 min in other processes. This shorter exposure likely resulted in fewer defects and less reduction in lateral size and thickness, allowing for more effective bonding with aluminum and promoting the grain refinement required during sintering. Although the grain size of the aluminum matrix was not quantified in this study, the literature suggests that the presence of well-dispersed carbon nanostructures, such as rGO, can act as nucleation sites or restrict the growth of matrix grains during sintering[60]. The preservation of the integrity and lateral dimensions of rGO, as inferred for the Mec-Stir method, would be determinative to maximize this grain refinement effect, thereby contributing to the observed increase in hardness, in accordance with the Hall-Petch relationship.

The Al/rGO composite mixed using a rotary evaporator showed a 15.9% increase in microhardness compared to pure aluminum. However, this performance may have been limited by the longer ultrasonication time required to disperse rGO, leading to defects and decreased lateral size and thickness. An advantage of the rotary evaporation method is the simultaneous mixing and evaporation of the solvent, which reduces processing time and potentially decreases the structural impact on rGO and GO.

In addition, the use of GO, regardless of the method, did not show such significant gains. These results highlight the importance of the choice of reinforcement (rGO versus GO) in addition to the processing method to optimize the mechanical properties of aluminum composites.

Besides the absolute gains in microhardness, the statistical analysis of the data reveals the importance of processing parameters for both the uniformity and effectiveness of the reinforcement. It was observed that the Al/rGO composite processed by mechanical stirring exhibited a significantly higher average microhardness (62.6 HV, a 60.5% increase over pure aluminum, which has 39.0 ± 1.5 HV), but with a standard deviation of 12.2 HV, indicating greater variability in reinforcement dispersion. In contrast, the composite obtained via rotary evaporation showed a more modest gain (45.2 HV, a 15.9% increase) with a standard deviation of only 3.5 HV, reflecting a more reproducible process, although less effective in enhancing the reinforcement.

These statistical results, when correlated with process parameters – such as ultrasonication time (15 min versus 30 min), stirring intensity, and evaporation conditions – suggest that optimizing processing conditions is critical not only for maximizing mechanical improvements but also for ensuring the homogeneous dispersion of rGO, which is crucial for efficient load transfer in the aluminum matrix. In summary, small variations in experimental parameters can significantly impact both the enhancement of properties and the reproducibility of the results. So, the choice of the mixing method, therefore, represents a balance between the energy supplied for dispersion and the potential damage to the reinforcing material, directly influencing the microstructure and the final mechanical properties of the composite.

Figures 6 and 7 show the scanning electron micrographs of the composites that demonstrated the best performance in the hardness test: Al/rGO (*Mec-Stir*) and Al/rGO (*Rot-Evap*), respectively.

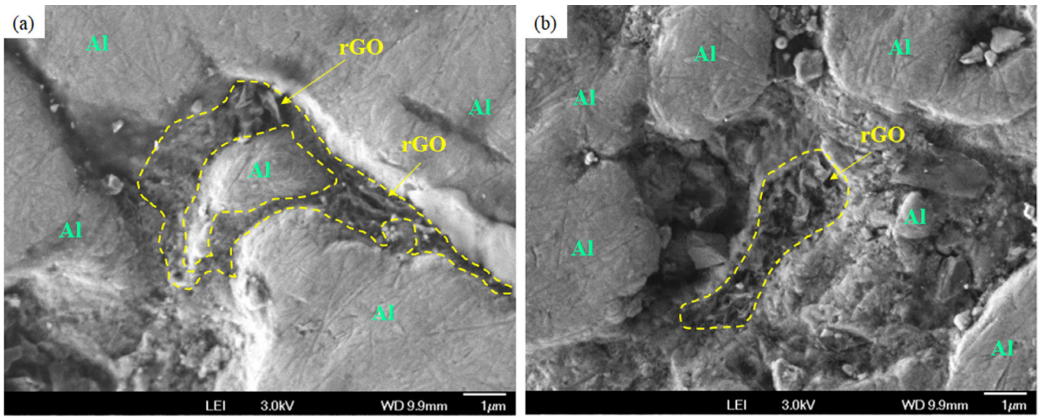

Figure 7. FEG-SEM of Al/rGO Composite (*Rot-Evap*): (a) aluminum region surrounded by rGO at grain boundaries; (b) rGO agglomerate encased by aluminum.

Post-sintering microstructural analysis, as shown in Figures 6 and 7, reveals important features of the composites. In Figure 6a, aluminum particles are surrounded by rGO layers, resulting in a rough surface texture due to the stacking of layered structures. Figures 6b, 6c, 7a, and 7b demonstrate that rGO is situated at the grain boundaries of the aluminum particles, aligning with observations from other studies[7,58,61]. Localized aggregation of folded and multilayered rGO may impede effective load transfer between the matrix and reinforcement because it is concentrated in specific areas. However, the distinct presence of well-defined rGO layers in Figures 7a and 7b indicates that some rGO remained intact during the rotary evaporation process. These findings suggest that rGO was successfully integrated into the composites using both methods, as evidenced in Figures 6 and 7, thus contributing to the enhancement of mechanical properties.

4. Conclusions

The main objective was achieved by comparing different graphene-based materials. The study aimed to identify an optimal liquid dispersion medium and evaluate various mixing techniques to establish a clear correlation between processing conditions, the integrity of graphene-based materials, and the resulting mechanical properties of the composites.:

- Solvent selection is critical for process viability. The initial evaluation demonstrated that aqueous media (water and ethanol/water mixtures) are unsuitable for this process. The use of water triggered a hydrolysis reaction with aluminum, forming aluminum hydroxide ($Al(OH)_3$), which was confirmed by XRD and SEM. This contamination hindered powder compaction and led to severe sample expansion during sintering due to the release of trapped water vapor, resulting in structurally unsound composites. In contrast, acetone and pure ethanol were identified as effective and inert media, producing high-density (>90%) sintered composites without deleterious reactions.
- The reinforcement type and mixing method determine mechanical performance. A clear distinction in performance was observed between the two reinforcements, with rGO consistently proving superior to GO for enhancing microhardness. The most significant result was achieved with the Al/rGO composite prepared by mechanical stirring (Mec-Stir), which exhibited a remarkable 60.5% increase in microhardness compared to pure aluminum. This success is attributed to a balanced processing approach, where a shorter initial ultrasonication period (15 min) was sufficient to deagglomerate the rGO without causing significant structural damage, allowing for effective reinforcement.
- Excessive processing energy is detrimental to reinforcement. The methods relying on prolonged, high-energy probe ultrasonication (Prob-Ult) yielded negligible improvements in hardness (<4%). This suggests that while sonication is effective for dispersion, excessive exposure leads to the fragmentation and degradation of the graphene sheets, rendering them ineffective for load transfer. The rotary evaporation (Rot-Evap) method provided a moderate hardness increase (15.9%), offering a reproducible process but likely causing more structural damage to the rGO than the gentler mechanical stirring.
- In-situ reduction of GO and carbide formation were confirmed. XRD and Raman analyses confirmed that GO was successfully reduced to rGO during the thermo-mechanical processing. However, the analysis also revealed the presence of aluminum carbide (Al_4C_3) peaks in all composites, indicating an interfacial reaction occurred during sintering, which is often associated with a negative impact on mechanical properties.

In conclusion, this work demonstrates that an effective Al/rGO composite can be fabricated by carefully controlling the energy input during mixing. The mechanical stirring method, combined with a brief initial sonication in an acetone medium, provides the optimal balance between achieving homogeneous dispersion and preserving the structural integrity of the rGO reinforcement, leading to a substantial enhancement in the composite's microhardness. The choice of the mixing technique is therefore a decisive factor that governs the final performance of Al-graphene composites produced by powder metallurgy.

5. Acknowledgement

The authors acknowledge the research support provided by Companhia Brasileira de Alumínio – CBA. Financial support from the Institutional Internationalization Project UPM/CAPES PrInt; CNPq Research Productivity Grant: 310204/2021-6; CNPq Universal Project: 407050/2023-0, and DAI/CNPq Project: 142558/2019-2 is also gratefully acknowledged. Additionally, we thank ZwickRoell Ltda. for providing the microhardness characterization equipment and Universidade Presbiteriana Mackenzie – UPM for their support.

6. References

1. Lee C, Wei X, Kysar JW, Hone J. Measurement of the elastic properties and intrinsic strength of monolayer graphene. Science. 2008;321(5887):385-8. https://doi.org/10.1126/science.1157996.
2. Chen Y, Zhang X, Liu E, He C, Shi C, Li J, et al. Fabrication of in-situ grown graphene reinforced Cu matrix composites. Sci Rep. 2016;6(1):19363. https://doi.org/10.1038/srep19363.
3. Rashad M, Pan F, Tang A, Asif M, She J, Gou J, et al. Development of magnesium-graphene nanoplatelets composite. J Compos Mater. 2015;49(3):285-93. https://doi.org/10.1177/0021998313518360.
4. Cao Z, Wang X, Li J, Wu Y, Zhang H, Guo J, et al. Reinforcement with graphene nanoflakes in titanium matrix composites. J Alloys Compd. 2017;696:498-502. https://doi.org/10.1016/j.jallcom.2016.11.302.
5. Wang J, Li Z, Fan G, Pan H, Chen Z, Zhang D. Reinforcement with graphene nanosheets in aluminum matrix composites. Scr Mater. 2012;66(8):594-7. https://doi.org/10.1016/j.scriptamat.2012.01.012.
6. Jiang L, Li Z, Fan G, Zhang D. A flake powder metallurgy approach to Al2O3/Al biomimetic nanolaminated composites with enhanced ductility. Scr Mater. 2011;65(5):412-5. https://doi.org/10.1016/j.scriptamat.2011.05.022.
7. Gao X, Yue H, Guo E, Zhang H, Lin X, Yao L, et al. Preparation and tensile properties of homogeneously dispersed graphene reinforced aluminum matrix composites. Mater Des. 2016;94:54-60. https://doi.org/10.1016/j.matdes.2016.01.034.
8. Bastwros M, Kim GY, Zhu C, Zhang K, Wang S, Tang X, et al. Effect of ball milling on graphene reinforced Al6061 composite fabricated by semi-solid sintering. Compos, Part B Eng. 2014;60:111-8. https://doi.org/10.1016/j.compositesb.2013.12.043.
9. Pérez-Bustamante R, Bolaños-Morales D, Bonilla-Martínez J, Estrada-Guel I, Martínez-Sánchez R. Microstructural and hardness behavior of graphene-nanoplatelets/aluminum composites synthesized by mechanical alloying. J Alloys Compd. 2014;615:S578-82. https://doi.org/10.1016/j.jallcom.2014.01.225.
10. Ju JM, Wang G, Sim KH. Facile synthesis of graphene reinforced Al matrix composites with improved dispersion of graphene and enhanced mechanical properties. J Alloys Compd. 2017;704:585-92. https://doi.org/10.1016/j.jallcom.2017.01.314.
11. Kumar HGP, Xavior MA. Graphene Reinforced Metal Matrix Composite (GRMMC): a review. Procedia Eng. 2014;97:1033-40. https://doi.org/10.1016/j.proeng.2014.12.381.
12. Bartolucci SF, Paras J, Reif J, Rafiee J, Lee S, Kapoor D, et al. Graphene–aluminum nanocomposites. Mater Sci Eng A. 2011;528(27):7933-7. https://doi.org/10.1016/j.msea.2011.07.043.
13. Zhou T, Lei M, Xu J. Recent progress in the development and properties of aluminum matrix composites reinforced with graphene: A review. Materials Today Sustainability. 2024;25:100674. https://doi.org/10.1016/j.mtsust.2024.100674.
14. Chak V, Chattopadhyay H. Fabrication and heat treatment of graphene nanoplatelets reinforced aluminium nanocomposites. Mater Sci Eng A. 2020;791:139657. https://doi.org/10.1016/j.msea.2020.139657.
15. Konios D, Stylianakis MM, Stratakis E, Kymakis E. Dispersion behaviour of graphene oxide and reduced graphene oxide. J Colloid Interface Sci. 2014;430:108-12. https://doi.org/10.1016/j.jcis.2014.05.033.
16. Naseer A, Ahmad F, Aslam M, Guan BH, Harun WSW, Muhamad N, et al. A review of processing techniques for graphene-reinforced metal matrix composites. Mater Manuf Process. 2019;34(9):957-85. https://doi.org/10.1080/10426914.2019.1615080.
17. Ghodrati H, Ghomashchi R. Effect of graphene dispersion and interfacial bonding on the mechanical properties of metal matrix composites: an overview. FlatChem. 2019;16:100113. https://doi.org/10.1016/j.flatc.2019.100113.
18. Tabandeh-Khorshid M, Omrani E, Menezes PL, Rohatgi PK. Tribological performance of self-lubricating aluminum matrix nanocomposites: role of graphene nanoplatelets. Eng Sci Technol Int J. 2016;19(1):463-9. https://doi.org/10.1016/j.jestch.2015.09.005.
19. Czeppe T, Korznikova E, Ozga P, Lityńska-Dobrzyńska L, Socha R. Application of the high pressure torsion supported by mechanical alloying for the metal-graphene composites preparation. Mechanik. 2015;(2):126-57. https://doi.org/10.17814/mechanik.2015.2.84.
20. Pillari LK, Shukla AK, Murty SVSN, Umasankar V. On the Comparison of graphene and multi-wall carbon nanotubes as reinforcements in aluminum alloy AA2219 processed by ball milling and spark plasma sintering. Trans Indian Inst Met. 2018;71(5):1099-112. https://doi.org/10.1007/s12666-017-1245-0.
21. Asgharzadeh H, Sedigh M. Synthesis and mechanical properties of Al matrix composites reinforced with few-layer graphene and graphene oxide. J Alloys Compd. 2017;728:47-62. https://doi.org/10.1016/j.jallcom.2017.08.268.
22. Dasari BL, Morshed M, Nouri JM, Brabazon D, Naher S. Mechanical properties of graphene oxide reinforced aluminium matrix composites. Compos, Part B Eng. 2018;145:136-44. https://doi.org/10.1016/j.compositesb.2018.03.022.
23. Bisht A, Srivastava M, Kumar RM, Lahiri I, Lahiri D. Strengthening mechanism in graphene nanoplatelets reinforced aluminum composite fabricated through spark plasma sintering. Mater Sci Eng A. 2017;695:20-8. https://doi.org/10.1016/j.msea.2017.04.009.
24. Latief FH, Sherif ESM, Almajid AA, Junaedi H. Fabrication of exfoliated graphite nanoplatelets-reinforced aluminum composites and evaluating their mechanical properties and corrosion behavior. J Anal Appl Pyrolysis. 2011;92(2):485-92. https://doi.org/10.1016/j.jaap.2011.09.003.
25. Wozniak J, Kostecki M, Cygan T, Buczek M, Olszyna A. Self-lubricating aluminium matrix composites reinforced with 2D crystals. Compos, Part B Eng. 2017;111:1-9. https://doi.org/10.1016/j.compositesb.2016.11.054.
26. Liu X, Fan YC, Feng Q, Wang LJ, Jiang W. Preparation of graphene nanosheet/alumina composites. Mater Sci Forum. 2013;745-746:534-8. https://doi.org/10.4028/www.scientific.net/MSF.745-746.534.
27. Whillock GOH, Harvey BF. Preliminary investigation of the ultrasonically enhanced corrosion of stainless steel in the nitric acid/chloride system. Ultrason Sonochem. 1996;3(2):S111-8. https://doi.org/10.1016/1350-1477(96)00002-U.
28. Huang XN, Lv CJ, Wang Y, Shen HY, Chen D, Huang YX. Hydrogen generation from hydrolysis of aluminum/graphite composites with a core–shell structure. Int J Hydrogen Energy. 2012;37(9):7457-63. https://doi.org/10.1016/j.ijhydene.2012.01.126.
29. Zhang L, Hou G, Zhai W, Ai Q, Feng J, Zhang L, et al. Aluminum/graphene composites with enhanced heat-dissipation properties by in-situ reduction of graphene oxide on aluminum particles. J Alloys Compd. 2018;748:854-60. https://doi.org/10.1016/j.jallcom.2018.03.237.

30. Wang HW, Chung HW, Teng HT, Cao G. Generation of hydrogen from aluminum and water – Effect of metal oxide nanocrystals and water quality. Int J Hydrogen Energy. 2011;36(23):15136-44. https://doi.org/10.1016/j.ijhydene.2011.08.077.
31. Zhang H, Zhang X, Graham TR, Pearce CI, Hlushko H, LaVerne JA, et al. Crystallization and phase transformations of aluminum (Oxy)hydroxide polymorphs in caustic aqueous solution. Inorg Chem. 2021;60(13):9820-32. https://doi.org/10.1021/acs.inorgchem.1c01111.
32. Deng Z, Fukasawa T, Ando M, Zhang G, Ohji T. High-surface-area alumina ceramics fabricated by the decomposition of $Al(OH)_3$. J Am Ceram Soc. 2001;84(3):485-91. https://doi.org/10.1111/j.1151-2916.2001.tb00687.x.
33. Bhattacharya IN, Das SC, Mukherjee PS, Paul S, Mitra PK. Thermal decomposition of precipitated fine aluminium trihydroxide. Scand J Metall. 2004;33(4):211-9. https://doi.org/10.1111/j.1600-0692.2004.00686.x.
34. Xie Y, Kocaefe D, Kocaefe Y, Cheng J, Liu W. The effect of novel synthetic methods and parameters control on morphology of nano-alumina particles. Nanoscale Res Lett. 2016;11(1):259. https://doi.org/10.1186/s11671-016-1472-z.
35. Hao H, Wang Y, Jafari Nodooshan HR, Zhang Y, Ye S, Lv Y, et al. The effects of sintering temperature and addition of TiH2 on the sintering process of Cu. Materials. 2019;12(16):2594. https://doi.org/10.3390/ma12162594.
36. Jiao X, Qiu Y, Zhang L, Zhang X. Comparison of the characteristic properties of reduced graphene oxides synthesized from natural graphites with different graphitization degrees. RSC Adv. 2017;7(82):52337-44. https://doi.org/10.1039/C7RA10809E.
37. Lesiak B, Trykowski G, Tóth J, Biniak S, Kövér L, Rangam N, et al. Chemical and structural properties of reduced graphene oxide: dependence on the reducing agent. J Mater Sci. 2021;56(5):3738-54. https://doi.org/10.1007/s10853-020-05461-1.
38. Li W, Cochell T, Manthiram A. Activation of aluminum as an effective reducing agent by pitting corrosion for wet-chemical synthesis. Sci Rep. 2013;3(1):1229. https://doi.org/10.1038/srep01229.
39. Li D, Müller MB, Gilje S, Kaner RB, Wallace GG. Processable aqueous dispersions of graphene nanosheets. Nat Nanotechnol. 2008;3(2):101-5. https://doi.org/10.1038/nnano.2007.451.
40. Li MJ, Liu CM, Xie YB, Cao HB, Zhao H, Zhang Y. The evolution of surface charge on graphene oxide during the reduction and its application in electroanalysis. Carbon. 2014;66:302-11. https://doi.org/10.1016/j.carbon.2013.09.004.
41. Li Z, Fan G, Tan Z, Guo Q, Xiong D, Su Y, et al. Uniform dispersion of graphene oxide in aluminum powder by direct electrostatic adsorption for fabrication of graphene/aluminum composites. Nanotechnology. 2014;25(32):325601. https://doi.org/10.1088/0957-4484/25/32/325601.
42. Fan Z, Wang K, Wei T, Yan J, Song L, Shao B. An environmentally friendly and efficient route for the reduction of graphene oxide by aluminum powder. Carbon. 2010;48(5):1686-9. https://doi.org/10.1016/j.carbon.2009.12.063.
43. Mellado C, Figueroa T, Baez R, Meléndrez M, Fernández K. Effects of probe and bath ultrasonic treatments on graphene oxide structure. Mater Today Chem. 2019;13:1-7. https://doi.org/10.1016/j.mtchem.2019.04.006.
44. Soltani T, Kyu Lee B. A benign ultrasonic route to reduced graphene oxide from pristine graphite. J Colloid Interface Sci. 2017;486:337-43. https://doi.org/10.1016/j.jcis.2016.09.075.
45. Rae J, Ashokkumar M, Eulaerts O, von Sonntag C, Reisse J, Grieser F. Estimation of ultrasound induced cavitation bubble temperatures in aqueous solutions. Ultrason Sonochem. 2005;12(5):325-9. https://doi.org/10.1016/j.ultsonch.2004.06.007.
46. Zhang W, He W, Jing X. Preparation of a stable graphene dispersion with high concentration by ultrasound. J Phys Chem B. 2010;114(32):10368-73. https://doi.org/10.1021/jp1037443.
47. Krishnamoorthy K, Kim GS, Kim SJ. Graphene nanosheets: ultrasound assisted synthesis and characterization. Ultrason Sonochem. 2013;20(2):644-9. https://doi.org/10.1016/j.ultsonch.2012.09.007.
48. Yan SJ, Dai SL, Zhang XY, Yang C, Hong QH, Chen JZ, et al. Investigating aluminum alloy reinforced by graphene nanoflakes. Mater Sci Eng A. 2014;612:440-4. https://doi.org/10.1016/j.msea.2014.06.077.
49. Acik M, Lee G, Mattevi C, Pirkle A, Wallace RM, Chhowalla M, et al. The role of oxygen during thermal reduction of graphene oxide studied by infrared absorption spectroscopy. J Phys Chem C Nanomater Interfaces. 2011;115(40):19761-81. https://doi.org/10.1021/jp2052618.
50. D'Angelo D, Bongiorno C, Amato M, Deretzis I, La Magna A, Fazio E, et al. Oxygen functionalities evolution in thermally treated graphene oxide featured by EELS and DFT calculations. J Phys Chem C Nanomater Interfaces. 2017;121(9):5408-14. https://doi.org/10.1021/acs.jpcc.7b00239.
51. Li G, Xiong B. Effects of graphene content on microstructures and tensile property of graphene-nanosheets / aluminum composites. J Alloys Compd. 2017;697:31-6. https://doi.org/10.1016/j.jallcom.2016.12.147.
52. Ma B, Wang J, Lee TH, Dorris SE, Wen J, Balachandran U. Microstructural characterization of Al4C3 in aluminum–graphite composite prepared by electron-beam melting. J Mater Sci. 2018;53(14):10173-80. https://doi.org/10.1007/s10853-018-2336-y.
53. Wang Y, Alsmeyer DC, McCreery RL. Raman spectroscopy of carbon materials: structural basis of observed spectra. Chem Mater. 1990;2(5):557-63. https://doi.org/10.1021/cm00011a018.
54. Nemanich RJ, Solin SA. First- and second-order Raman scattering from finite-size crystals of graphite. Phys Rev B Condens Matter. 1979;20(2):392-401. https://doi.org/10.1103/PhysRevB.20.392.
55. Dresselhaus MS, Dresselhaus G. Intercalation compounds of graphite. Adv Phys. 1981;30(2):139-326. https://doi.org/10.1080/00018738100101367.
56. Bowling RJ, Packard RT, McCreery RL. Activation of highly ordered pyrolytic graphite for heterogeneous electron transfer: relationship between electrochemical performance and carbon microstructure. J Am Chem Soc. 1989;111(4):1217-23. https://doi.org/10.1021/ja00186a008.
57. Ferrari AC. Raman spectroscopy of graphene and graphite: Disorder, electron–phonon coupling, doping and nonadiabatic effects. Solid State Commun. 2007;143(1-2):47-57. https://doi.org/10.1016/j.ssc.2007.03.052.
58. Li JL, Xiong YC, Wang XD, Yan SJ, Yang C, He WW, et al. Microstructure and tensile properties of bulk nanostructured aluminum/graphene composites prepared via cryomilling. Mater Sci Eng A. 2015;626:400-5. https://doi.org/10.1016/j.msea.2014.12.102.
59. Baig Z, Mamat O, Mustapha M, Mumtaz A, Munir KS, Sarfraz M. Investigation of tip sonication effects on structural quality of graphene nanoplatelets (GNPs) for superior solvent dispersion. Ultrason Sonochem. 2018;45:133-49. https://doi.org/10.1016/j.ultsonch.2018.03.007.
60. Jayaseelan J, Pazhani A, Michael AX, Paulchamy J, Batako A, Hosamane Guruswamy PK. Characterization studies on graphene-aluminium nano composites for aerospace launch vehicle external fuel tank structural application. Materials. 2022;15(17):5907. https://doi.org/10.3390/ma15175907.
61. Zhang H, Xu C, Xiao W, Ameyama K, Ma C. Enhanced mechanical properties of Al5083 alloy with graphene nanoplates prepared by ball milling and hot extrusion. Mater Sci Eng A. 2016;658:8-15. https://doi.org/10.1016/j.msea.2016.01.076.

Data Availability

All data generated or analyzed during this study are included in this published article.